Geometric Evaluation of Balance Regions for Multi-Contact Humanoids Using Contact Stability Criteria

Saeid Samadi, Wenqian Du, and Sethu Vijayakumar

***Abstract*— In robotics research, geometric representations are often utilized to model the kinematics and dynamics of robots. One important application is achieving balance in real-time multi-contact scenarios with humanoid robots, which is challenging due to the high computational cost of multi-contact balance control strategies. In this paper, we propose a Chebyshev center method whole-body execution of real-time balance control that leverages contact stability criteria. Our approach provides insights into the potential of using geometric methods for real-time multi-contact balancing. Specifically, we demonstrate the relationship between contact stability and balance criteria in quasi-static motion, compare our method with literature that computes balance regions explicitly, and evaluate the correctness of our approach by demonstrating the resulting center of mass position within the relevant geometric region.**

I. Introduction

Humanoid robots are designed to perform tasks that involve human-like movements and function in unpredictable situations. However, unlike locomotion algorithms that consider Zero-tilting Moment Point (ZMP) assuming co-planar surface contacts, real-world applications require multi-contact configurations that present unique challenges. Achieving balance in a multi-contact motion requires selecting appropriate contact points, determining suitable body configurations, and considering motion constraints within a whole-body controller framework. This paper investigates real-time multi-contact balance control with a focus on evaluating balance regions based on contact stability.

Various models for different contact modes, such as fixed [1], [2], sliding [3], [4], soft [5], and rolling [6], have been presented to achieve tasks that require multi-contact configurations. Balance in multi-contact conditions has been mainly studied theoretically but only for non-sliding contacts [7]. Recent studies have proposed models to ensure the balance during multi-contact scenarios on non-coplanar surfaces, including the control of wrench distribution, modeling of error compensation, and adaptation of actual contact states with the environment. Enforcing dynamic balance for multi-legged robots in multi-contact scenarios can be achieved through computing the ZMP [8], center of mass (CoM) support regions [9], and gravito-inertial wrench cones (GIWC) [10]. However, these approaches require heavy computation of the respective balance regions.

In order to achieve active balance in various scenarios, humanoid robots require a well-planned approach for contact placements and corresponding whole-body motion. To this end, various whole-body control strategies have been proposed in literature that prioritize task-space controllers using different order-based schemes, such as strict [11], weighted [12], or hybrid [13] priority. These strategies are formulated as Quadratic Programming (QP) problems, where tasks are either formulated as cost functions or constraints.

Centroidal momentum control (CMC) has become a popular approach for achieving robust whole-body control of humanoid robots in the presence of disturbances, as it can better handle unanticipated perturbations compared to inverse-dynamics controllers [14]. However, CMC is computationally expensive, especially for hybrid-dynamics models that account for the dynamics of both the rigid-body system and the environment [15]. To mitigate this computational burden, simplified dynamical models such as centroidal dynamics have been proposed [16].

Motion planners generate proper distribution of wrenches based on the centroidal model, while whole-body balance controllers maintain balance by realizing these wrenches on the robot and mapping contact forces into joint positions [17] or torques [5]. Inverse kinematics techniques are utilized to obtain joint commands for the desired CoM trajectory and body configuration

Our proposed approach for real-time multi-contact balancing of humanoid robots is based on the principles of contact stability and quasi-static motion. By leveraging these concepts, we have developed a balance control strategy that provides a conservative yet effective solution for achieving balance in challenging scenarios with multiple contacts. Our contributions to this problem are significant and multifaceted as follows:

- Studying a novel balance control strategy based on the Chebyshev center method for real-time multi-contact scenarios introduced in [18],
- Validation of the effectiveness of our proposed approach by comparing balance conditions to literature that computes geometric balance regions explicitly,
- Investigation of the relationship between contact stability and balance criteria in quasi-static motion and its implications for achieving balance in multi-contact scenarios,
- Demonstration of the effectiveness of the proposed approach through the computation of the balancing CoM position of the robot within the relevant CoM region based on publications that consider the explicit computation of geometric regions.

authors are with University of Edinburgh, UK. Corresponding author: ssamadi@ed.ac.uk

II. Radius Denotation in Balance Regions

Our previous work [18] used the Chebyshev method to achieve real-time balance in multi-contact scenarios, which bypasses the need for constructing balance regions, leading to high computational efficiency while maintaining conservativeness. To investigate the relationship between computed properties, such as the Chebyshev radius, and the balance region, we analyze the problem more specifically.

A. Dynamic and Contact Stabilities

We can represent the equation of motion for a robot with point or surface contacts with the environment as follows:

$$\mathbf{M}(\mathbf{q})\ddot{\mathbf{q}} + \mathbf{h}(\mathbf{q}, \dot{\mathbf{q}}) = \mathbf{S}^T\boldsymbol{\tau}_a + \sum_{contact\ i} \mathbf{J}_i^T\boldsymbol{\omega}_i. \tag{1}$$

Here, $\mathbf{q}$, $\dot{\mathbf{q}}$, and $\ddot{\mathbf{q}}$ are the vectors of degrees of freedom (DOF), $\mathbf{h}(\mathbf{q}, \dot{\mathbf{q}})$ is the vector of gravity and Coriolis forces, $\boldsymbol{\tau}_a$ is the vector of torques at the actuated joints, and $\mathbf{S}$ is the selection matrix. Additionally, $\boldsymbol{\omega}_i$ denotes the contact wrench taken with respect to a single contact point C_i on link i, while $\mathbf{J}_i$ denotes the $6 \times n$ matrix obtained by vertically stacking the translation and rotation jacobians, where n is the number of DOF.

1) Dynamic Equilibrium: A robot system comprises interconnected links forming a kinematic chain. The system's linear momentum, $\mathbf{P}$, and angular momentum, $\mathbf{L}_{CoM}$, are defined by:

$$\mathbf{P} \coloneqq \frac{1}{m}\sum_{link\ k} m_i\dot{\boldsymbol{c}}_i, \tag{2}$$

$$\mathbf{L}_{CoM} \coloneqq \sum_{link\ k} m_i(\mathbf{p}_i - \boldsymbol{c}) \times \dot{\boldsymbol{c}}_i + \mathbf{I}_i\boldsymbol{\omega}_i, \tag{3}$$

where $\mathbf{I}_i$ and $\boldsymbol{\omega}_i$ represent the inertial matrix and angular velocity of the link in the absolute frame, respectively, and $\boldsymbol{c}$ and $\boldsymbol{p}_i$ denote the positions of the robot's CoM and links, respectively. The robot's *dynamic wrench* at the CoM is defined as the wrench $(\dot{\mathbf{P}},\ \dot{\mathbf{L}}_{CoM})$, which can be obtained via forward kinematics from joint-angle positions, velocities, and accelerations. The *dynamic wrench* of the robot is equivalent to the total wrench of forces acting on the system, given by:

$$\begin{bmatrix}\dot{\mathbf{P}}\\ \dot{\mathbf{L}}_{CoM}\end{bmatrix} = \begin{bmatrix}\mathbf{f}^g\\ 0\end{bmatrix} + \sum_{contact\ i}\begin{bmatrix}\mathbf{f}_i\\ (\mathbf{p}_i - \boldsymbol{c}) \times \mathbf{f}_i\end{bmatrix}, \tag{4}$$

where $\mathbf{f}^g$ is the gravity force acting on the CoM. This equation is also known as *dynamic balance* or *dynamic equilibrium* of the system. The *Gravito-Inertial Wrench* (GIW) $\boldsymbol{w}^{gi}$ is defined with respect to a fixed point O as follows:

$$\boldsymbol{w}_O^{gi} \coloneqq \begin{bmatrix}\mathbf{f}^{gi}\\ \boldsymbol{\tau}_O^{gi}\end{bmatrix} \coloneqq \begin{bmatrix}\mathbf{f}^g - \dot{\mathbf{P}}\\ (\boldsymbol{c} - \mathbf{p}_O) \times (\mathbf{f}^g - \dot{\mathbf{P}}) - \dot{\mathbf{L}}_{CoM}\end{bmatrix}, \tag{5}$$

whereas the contact wrench $\boldsymbol{w}^c$ is represented as:

$$\boldsymbol{w}_O^c \coloneqq \begin{bmatrix}\mathbf{f}^c\\ \boldsymbol{\tau}_O^c\end{bmatrix} \coloneqq \sum_{contact\ i}\begin{bmatrix}\mathbf{f}\\ \mathbf{p}_i \times \mathbf{f}_i\end{bmatrix}. \tag{6}$$

Therefore, the system's *dynamic equilibrium* or *balance* can be expressed as

$$\boldsymbol{w}^{gi} + \boldsymbol{w}^c = 0. \tag{7}$$

The formulation known as the *wrench-space* equilibrium, expressed as Eq. (7), is used to describe dynamic balance in robotics. This formulation is based on the separation of the overall system's motion into two components:

- The *gravito-inertial wrench*, which describes the system's self-motion.
- The *contact wrench*, which describes the system's interaction with its environment.

2) Contact Stability: Humanoid robots can achieve stability in multi-contact scenarios by satisfying the contact stability criterion, as described in [19] and [20]. This involves finding a solution $(\ddot{\boldsymbol{q}},\ \boldsymbol{\tau},\ \boldsymbol{w}_1,\ ...,\ \boldsymbol{w}_n)$ of the equations of motion that meets the contact mode for all contacting links, ensuring that the contacting link has no relative motion, torque limits are satisfied, and contact wrenches are within their respective Contact Wrench Cone (CWC).

Since local contact wrenches lie in wrench cones, the whole-body wrench cone must also be within the CWC. The general multi-contact stability criterion states that the robot's motion is weak-contact stable if the contact wrench it generates belongs to the CWC (resp. GIWC).

B. Calculation of the Range of Contact Wrench

The optimization problem in [18] provides the Chebyshev radius, which represents a range for all contact wrenches. However, we need to calculate the range of the gravito-inertial wrench within the GIWC based on this radius. This involves incorporating the radius into the computation process of the GIWC. Note that the contact wrench cone is simply the opposite of the GIWC. Therefore, we need to consider both whole-body contact and gravito-inertial wrenches when calculating the range. Assuming a set of contact wrenches expressed at the CoM within their respective contact wrench cones $\boldsymbol{w}_i \in \mathcal{C}_i$ for $i = 1, \ldots, l$, we can represent the Chebyshev method as follows:

$$\boldsymbol{w}_i + r\boldsymbol{a} \in \mathcal{C}_i. \tag{8}$$

We can then express the sum of contact wrenches and their ranges $(r\boldsymbol{a})$ as:

$$\sum_{i=1}^{l} \boldsymbol{w}_i + lr\boldsymbol{a} \in \mathcal{C}_1 \oplus \ldots \oplus \mathcal{C}_l. \tag{9}$$

Here, $\oplus$ denotes the Minkowski sum of the contact wrench cones, which explicitly defines the CWC. Therefore, the range for valid whole-body contact and gravito-inertial wrenches is a sphere with a radius of:

$$r_{cwc} = lr. \tag{10}$$

To explain why we need to implement the Minkowski sum, we will provide a numerical example in the following section.

1) Numerical Example: We present a numerical example to illustrate the Minkowski sum concept. In this example, we consider two contact points in 3D space, as shown as blue planes in Fig. 2, along with their associated convex polyhedra and contact forces. The friction coefficients of the contacts are $\mu_1 = 0.5$ and $\mu_2 = 0.35$, respectively. Fig. 1(b) illustrates the corresponding friction cones according to the friction coefficients. It is worth mentioning that the friction cones are in vector space, which we omitted to avoid making the figure too complex.

We set the CoM position to $\mathbf{p}_G = [0 \quad 0 \quad 0.6]^T$. The location of the polyhedra and forces is then shifted according to the CoM position, as shown in Fig. 1(a). Here, the Minkowski sum of the contact polyhedra forms the polyhedron at the CoM position. To illustrate the CWC, we depict the forces that lie on the edge of the corresponding friction cone. These forces are then translated to the CoM position, and the resultant force is shown in Fig. 1(a). We ensured that the friction cones have ceilings by considering the upper limit for the normal force during the calculation of the friction cones. The computed wrench and Chebyshev radius result in spheres for all contacts, as depicted in Fig. 1(b). The larger sphere inside the CWC has a radius equal to twice the Chebyshev radius, which is always located inside the CWC, demonstrating the conservativeness of our approach.

C. Calculation of the Range of CoM Position

We seek to convert the Chebyshev radius into the static equilibrium region and determine the range for the CoM position. Initially, we define the CWC, $\mathbf{W}$, at a fixed point O as per inequality Eq. (11):

$$\mathbf{A}_O \mathbf{W}_O \leqslant \mathbf{0}. \tag{11}$$

We use the Chebyshev range, r_{cwc}, for the i-th row of A_O based on section II-B. This results in the following inequality:

$$\mathbf{A}_{O,i} \mathbf{W}_O + r_{cwc} \left\| \mathbf{A}_{O,i} \right\| \leqslant b_i. \tag{12}$$

By using the *dual twist* representation of the inequality from [21] and with $\mathbf{W}_O = [\boldsymbol{f} \quad \boldsymbol{\tau}_O]^T$, we can re-write the above equation as

$$\mathbf{a}_O.\mathbf{f} + \mathbf{a}.\boldsymbol{\tau}_O + r_{cwc} \left\| \mathbf{A}_{O,i} \right\| \leqslant b_i, \tag{13}$$

where $\boldsymbol{a}_O = [a_{Ox} \quad a_{Oy} \quad a_{Oz}]^T$ and $\boldsymbol{a} = [a_x \quad a_y \quad a_z]^T$. By considering static equilibrium ($\boldsymbol{\tau}_G = \mathbf{0}$ and $\mathbf{f} = m\mathbf{g}$) and representing the inequality at point G, we continue the calculation as following:

$$\begin{aligned}
m(\mathbf{a}_O + \mathbf{a} \times \mathbf{p}_G).\mathbf{g} + r_{cwc} \left\| \mathbf{A}_{O,i} \right\| &\leqslant b_i, \\
-mg(\mathbf{a}_{Oz} - \mathbf{a}_y x_G + \mathbf{a}_x y_G) + r_{cwc} \left\| \mathbf{A}_{O,i} \right\| &\leqslant b_i, \\
\frac{-1}{\left\| \mathbf{A}_{O,i} \right\|}(\mathbf{a}_{Oz} - \mathbf{a}_y x_G + \mathbf{a}_x y_G) + \frac{r_{cwc}}{mg} &\leqslant \frac{b_i}{mg \left\| \mathbf{A}_{O,i} \right\|}, \\
\frac{-1}{\left\| \mathbf{A}_{O,i} \right\|}(\mathbf{a}_{Oz} - \mathbf{a}_y x_G + \mathbf{a}_x y_G) - \frac{b_i}{mg \left\| \mathbf{A}_{O,i} \right\|} &\leqslant -\frac{r_{cwc}}{mg}.
\end{aligned}$$

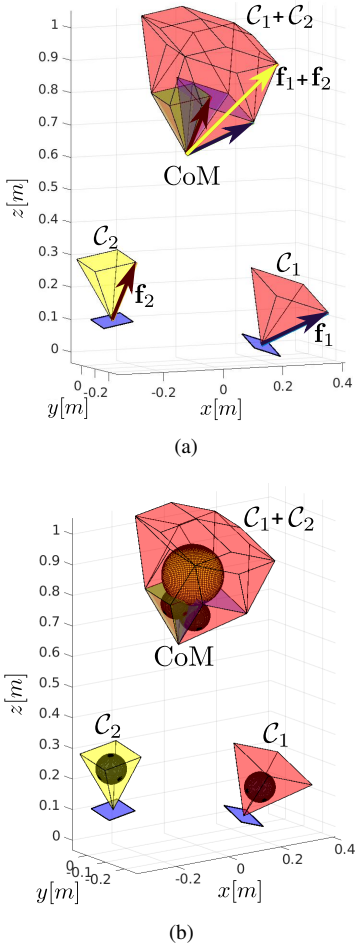

Fig. 1. Minkowski sum of friction cones at CoM position, illustrating (a) forces lying on the edges of cones and their translated sum, and (b) computed wrenches and Chebyshev radius resulting in spheres. The larger sphere's radius is equal to the sum of the smaller ones.

Without loss of generality, we can assume $\left\| \mathbf{A}_{O,i} \right\| = 1$. So, the inequality Eq. (11) becomes:

$$-(\mathbf{a}_{Oz} - \mathbf{a}_y x_G + \mathbf{a}_x y_G - \frac{b_i}{mg}) \leqslant -\frac{r_{cwc}}{mg}. \tag{14}$$

We denote the signed distance between $(x_G,\ y_G)$ and the supporting line $-\mathbf{a}_{Oz} + \mathbf{a}_y x_G - \mathbf{a}_x y_G + \frac{b_i}{mg} = 0$ of the corresponding equilibrium polygon's edge as

$$\sigma_{A,i}(x_G,\ y_G) = \mathbf{a}_{Oz} - \mathbf{a}_y x_G + \mathbf{a}_x y_G - \frac{b_i}{mg}. \tag{15}$$

The inequality presented above implies that the distance between the CoM and the boundaries of the static equilibrium region (as defined in [9]) is at least $r_{com} = \frac{r_{cwc}}{mg}$.

III. Experimental Validation

In our simulation validation, we investigate a multi-contact scenario similar to the one executed in our recent work [18]. The robot is initially in a non-coplanar multi-contact configuration and steps up a slope to make contact with a tilted board and a vertical wall, followed by executing a co-wiping motion. A video reference is available for further details[1].

[1] https://youtu.be/cFYd9oQueRE

Using the computation method presented in Section II-C, we are able to compute the range of a conservative CoM region within the quasi-static balance region. This is achieved by using the computed Chebyshev radius during the execution and displaying the CoM range geometrically as a circle with a variable radius. The radius ensures that all points inside the circle, including the CoM output, which is the center of the circle (known as the Chebyshev center), will remain inside the balance region.

The static balance region is computed based on [9]. Also, There are three different CoM positions displayed in the following figures. The green CoM is the output of the optimization problem that is solved using the Chebyshev center method and serves as the target for the whole-body to track. The yellow CoM is the output of the whole-body QP, which aims to track the reference (green) CoM. Finally, the blue CoM is the computed CoM based on the estimators and is labeled as the real CoM.

The simulation of the motion of the CoM within the geometric balance region is available[1]. Moreover, we are using mc_rtc framework[2] for execution of the motion. Please note that the proposed balance control strategy focuses on quasi-static motions and does not consider breaking and making contacts. As a result, in order to reach the desired configuration, we initially use existing methods to step up the slope. This can be observed in Fig. 2(b), where the tracking CoM (shown as a blue dot) is noticeably different from the output of the Chebyshev QP (shown as a green dot).

We have conducted simulations to validate the effectiveness of our approach in achieving balance within the geometric balance region. To execute the motion, we utilized the mc_rtc framework, which allows us to specify the motions in task space and solves for the whole-body motion of the robot using its embedded QP solver. Our simulations demonstrated that the robot's CoM remained within the geometric balance region during multi-contact motion, validating the effectiveness of our approach and computations of section Section II-C.

IV. Conclusion

In this research, we studied a Chebyshev center method for achieving real-time balance in multi-contact scenarios with humanoid robots. Our approach is based on leveraging contact stability criteria and provides insights into the potential of using geometric methods for multi-contact balancing. We investigated the relationship between contact stability and balance criteria in quasi-static motion and compared our approach with literature that computes balance regions geometrically. To validate our approach and demonstrate its effectiveness in maintaining balance, we presented the resulting CoM position of the robot and the conservative estimate of the balance region using the calculations provided in section Section II-C, which is consistent with previous literature. Our findings suggest that the Chebyshev center method can provide a conservative yet effective solution for real-time multi-contact balancing in humanoid robots.

[1]https://youtu.be/_Ui4AGhS_7Q
[2]https://github.com/jrl-umi3218/mc_rtc

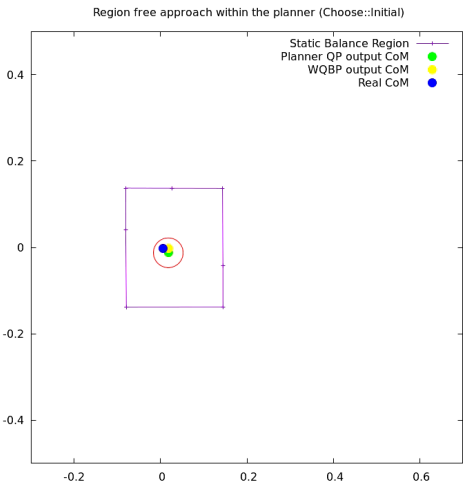

(a)

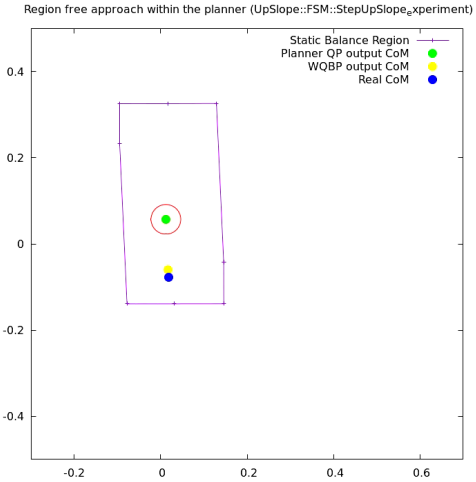

(b)

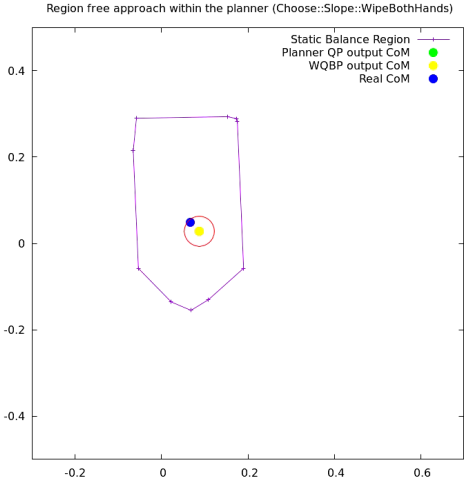

(c)

Fig. 2. Demonstration of the CoM position and conservative region as a circle computed in section Section II-C within the static balance region computed based on [9]. Figures (a), (b), and (c) show the initial state, stepping up the slope, and the co-wiping motion, respectively.

REFERENCES

[1] N. Hiraoka, M. Murooka, S. Noda, K. Okada, and M. Inaba, "Online generation and control of quasi-static multi-contact motion by pwt jacobian matrix with contact wrench estimation and joint load reduction*," *Advanced Robotics*, vol. 35, no. 1, pp. 48–63, 2021.

[2] M. P. Polverini, A. Laurenzi, E. M. Hoffman, F. Ruscelli, and N. G. Tsagarakis, "Multi-contact heavy object pushing with a centaur-type humanoid robot: Planning and control for a real demonstrator," *IEEE Robotics and Automation Letters*, vol. 5, no. 2, pp. 859–866, 2020.

[3] S. Samadi, S. Caron, A. Tanguy, and A. Kheddar, "Balance of humanoid robots in a mix of fixed and sliding multi-contact scenarios," in *IEEE International Conference on Robotics and Automation*, pp. 6590–6596, 2020.

[4] J. Shi, J. Z. Woodruff, P. B. Umbanhowar, and K. M. Lynch, "Dynamic In-Hand Sliding Manipulation," *IEEE Transactions on Robotics*, vol. 33, no. 4, pp. 778–795, 2017.

[5] B. Henze, M. A. Roa, and C. Ott, "Passivity-based whole-body balancing for torque-controlled humanoid robots in multi-contact scenarios," *The International Journal of Robotics Research*, vol. 35, no. 12, pp. 1522–1543, 2016.

[6] M. Murooka, I. Kumagai, M. Morisawa, F. Kanehiro, and A. Kheddar, "Humanoid loco-manipulation planning based on graph search and reachability maps," *IEEE Robotics and Automation Letters*, vol. 6, no. 2, pp. 1840–1847, 2021.

[7] C. Collette, A. Micaelli, C. Andriot, and P. Lemerle, "Dynamic balance control of humanoids for multiple grasps and non coplanar frictional contacts," in *IEEE-RAS International Conference on Humanoid Robots*, pp. 81–88, 2007.

[8] S. Caron, Q. C. Pham, and Y. Nakamura, "ZMP support areas for multicontact mobility under frictional constraints," *IEEE Transactions on Robotics*, vol. 33, no. 1, pp. 67–80, 2017.

[9] T. Bretl and S. Lall, "Testing static equilibrium for legged robots," *IEEE Transactions on Robotics*, vol. 24, no. 4, pp. 794–807, 2008.

[10] F. Abi-Farraj, B. Henze, C. Ott, P. R. Giordano, and M. A. Roa, "Torque-Based Balancing for a Humanoid Robot Performing High-Force Interaction Tasks," *IEEE Robotics and Automation Letters*, vol. 4, no. 2, pp. 2023–2030, 2019.

[11] A. Sherikov, D. Dimitrov, and P.-B. Wieber, "Balancing a humanoid robot with a prioritized contact force distribution," in *International Conference on Humanoid Robots*, pp. 223–228, IEEE, 2015.

[12] Y. Lee, S. Kim, J. Park, N. Tsagarakis, and J. Lee, "A whole-body control framework based on the operational space formulation under inequality constraints via task-oriented optimization," *IEEE Access*, vol. 9, pp. 39813–39826, 2021.

[13] M. Liu, R. Lober, and V. Padois, "Whole-body hierarchical motion and force control for humanoid robots," *Autonomous Robots*, vol. 40, no. 3, pp. 493–504, 2016.

[14] D. E. Orin, A. Goswami, and S.-H. Lee, "Centroidal dynamics of a humanoid robot," *Autonomous robots*, vol. 35, no. 2, pp. 161–176, 2013.

[15] M. Neunert, M. Stäuble, M. Giftthaler, C. D. Bellicoso, J. Carius, C. Gehring, M. Hutter, and J. Buchli, "Whole-body nonlinear model predictive control through contacts for quadrupeds," *IEEE Robotics and Automation Letters*, vol. 3, no. 3, pp. 1458–1465, 2018.

[16] H. Dai, A. Valenzuela, and R. Tedrake, "Whole-body motion planning with centroidal dynamics and full kinematics," in *IEEE-RAS International Conference on Humanoid Robots*, pp. 295–302, IEEE, 2014.

[17] K. Bouyarmane, K. Chappellet, J. Vaillant, and A. Kheddar, "Quadratic Programming for Multirobot and Task-Space Force Control," *IEEE Transactions on Robotics*, vol. 35, no. 1, pp. 64–77, 2019.

[18] S. Samadi, J. Roux, A. Tanguy, S. Caron, and A. Kheddar, "Humanoid control under interchangeable fixed and sliding unilateral contacts," *IEEE Robotics and Automation Letters*, vol. 6, no. 2, pp. 4032–4039, 2021.

[19] S. Caron, *Computational Foundation for Planner-in-the-Loop Multi-Contact Whole-Body Control of Humanoid Robots*. PhD thesis, University of Tokyo, 2015.

[20] J. S. Pang and J. Trinkle, "Stability characterizations of rigid body contact problems with Coulomb friction," *ZAMM Zeitschrift fur Angewandte Mathematik und Mechanik*, vol. 80, no. 10, pp. 643–663, 2000.

[21] S. Caron and A. Kheddar, "Multi-contact walking pattern generation based on model preview control of 3d com accelerations," in *IEEE-RAS International Conference on Humanoid Robots*, pp. 550–557, 2016.